Electronic Supplementary Material

Engineering HEA/CN Schottky Heterojunction with High-Entropy and Cocktail Effects for Enhanced Charge Separation in Photocatalytic Xylose Oxidation

Zhe Zheng [a], Yushun Han [a], Weikang Ling [a], Min Hong [b], Jiliang Ma *[a], and Runcang Sun [a]

[a] Liaoning Key Lab of Lignocellulose Chemistry and Bio-Materials, Liaoning Collaborative Innovation Center for Lignocellulosic Biorefinery, College of Light Industry and Chemical Engineering, Dalian Polytechnic University, Dalian 116034, China

[b] School of Engineering and Centre for Future Materials, University of Southern Queensland, Springfield Central Queensland 4300, Australia

*Corresponding authors' E-mail address: jlma@dlpu.edu.cn (Jiliang Ma), Tel.: +86-0411-86323652, Fax: +86-0411-86323652.

1. Experimental section

1.1. Characterization

The samples were characterized by a variety of techniques to investigate their physicochemical properties. The microstructure and morphology were observed using scanning electron microscopy (SEM, Hitachi S-4800) and transmission electron microscopy (TEM, JEM-2100 CXII). The specific surface area and pore structure were determined by N_2 adsorption-desorption measurements at 77 K using a physisorption analyzer (Micromeritics, ASAP 2020). The Brunauer-Emmett-Teller (BET) method was employed to calculate the specific surface area. Prior to analysis, all samples were degassed under vacuum at 200 ^{o}C for 12 h. The crystal structure was examined by X-ray diffraction (XRD, Bruker D8 Focus) using Cu Kα radiation (λ = 0.15418 nm), operated at 40 kV and 40 mA, with a scanning range (2θ) of 10-80^{o}. Fourier transform infrared (FT-IR) spectra of all samples were acquired on a Bruker Tensor 27 spectrometer within the measurement range of 400-4000 cm^{-1} at a resolution of 4 cm^{-1}.The samples were characterized by a variety of techniques to investigate their physicochemical properties. The microstructure and morphology were observed using scanning electron microscopy (SEM, Hitachi S-4800) and transmission electron microscopy (TEM, JEM-2100 CXII). The specific surface area and pore structure were determined by N_2 adsorption-desorption measurements at 77 K using a physisorption analyzer (Micromeritics, ASAP 2020). The Brunauer-Emmett-Teller (BET) method was employed to calculate the specific surface area. Prior to analysis, all samples were degassed under vacuum at 200 ^{o}C for 12 h. The crystal structure was examined by X-ray diffraction (XRD, Bruker D8 Focus) using Cu Kα radiation (λ = 0.15418 nm), operated at 40 kV and 40 mA, with a scanning range (2θ) of 10-80^{o}.The chemical states

and electronic structure were analyzed by X-ray photoelectron spectroscopy (XPS, Kratos Axis Ultra DLD) with a monochromatic Al Kα X-ray source (1486.6 eV). Ultraviolet-visible diffuse reflectance spectroscopy (UV-vis DRS) was performed on a U-3900 spectrophotometer in the range of 200-800 nm. Ultraviolet photoelectron spectroscopy (UPS) measurements were carried out using a He I light source (21.20 eV) and a VG Scienta R4000 analyzer. A sample bias of -5 V was applied to determine the secondary electron cutoff edge (E_{seco}), and the work function was calculated from the difference between the photon energy (21.20 eV) and the binding energy of the secondary cutoff edge. Photoluminescence (PL) spectra and time-resolved photoluminescence (TRPL) spectra were acquired at room temperature using an Edinburgh FLS-920 spectrofluorometer and an FLS1000 fluorescence lifetime spectrophotometer (excitation wavelength of 375 nm), respectively. Electron spin resonance (ESR) spectroscopy was used to detect unpaired electrons. 5,5-Dimethyl-1-pyrroline *N*-oxide (DMPO) was employed as a spin trap for detecting hydroxyl radicals (·OH), and 2,2,6,6-tetramethylpiperidine-1-oxyl (TEMPO) was used to characterize electrons and holes.

1.2. Photoelectrochemical Measurements

Electrochemical measurements were conducted using a CHI660E electrochemical workstation (Chen hua, China) with a conventional three-electrode configuration. A platinum (Pt) wire served as the counter electrode, and a saturated Ag/AgCl electrode was employed as the reference electrode. Fluorine-doped tin oxide (FTO) glass, after thorough cleaning, was utilized as the working electrode substrate. To prepare the working electrode, 5 mg of the target photocatalyst was dispersed in a mixture containing 20 μL of Nafion solution (5 wt%) and 0.98 mL of absolute ethanol. This

mixture was subjected to ultrasonic treatment for 30 minutes to form a homogeneous ink. The resulting suspension was then uniformly coated onto the pre-cleaned FTO substrate and allowed to dry. The electrochemical tests were performed in a 0.5 M Na_2SO_4 aqueous solution (pH = 6.8) as the supporting electrolyte. A 300 W Xe lamp was used as the visible light source to illuminate the electrode during photoelectrochemical measurements. Electrochemical impedance spectroscopy (EIS) was measured under illumination by applying an AC voltage amplitude of 10 mV at a DC bias of -0.3 V (vs. Ag/AgCl), scanning over a frequency range from 10 kHz to 0.01 Hz. Mott-Schottky analysis was carried out in the same electrolyte (0.5 M Na_2SO_4) at AC frequencies of 500, 800, and 1000 Hz with an amplitude of 5 mV.

1.3. Poisoning experiments

The photocatalytic experiments were conducted in a 50 mL quartz reactor. The reaction system consisted of 200 mg of xylose, 10 mg of the H/C-15 catalyst, and 20 mmol of an inhibitor, dispersed in 20 mL of a 0.2 M KOH aqueous solution. Prior to the reaction, the system was purged with CO_2 gas to remove air. Under constant stirring and maintained at 60 ^oC, the mixture was irradiated for 2 h using a visible light lamp (Model: Perfectlight PCX 50C; Power: 10 W; Light Intensity: 790 mW/cm^2). After the reaction, the products were analyzed according to established analytical methods.

1.4. Cycling experiment

A mixture of 200 mg xylose and 10 mg of the H/C-15 catalyst was dissolved in 20 mL of a 0.2 M KOH aqueous solution. The resulting mixture was subjected to ultrasonic treatment for approximately 2 minutes to ensure homogeneity and then transferred into a quartz reaction vessel. The reaction was conducted at 60 ^oC under irradiation from a 10 W LED light source for 2 h. After the reaction, the solid catalyst was recovered

through filtration and washed thoroughly. Finally, the H/C-15 catalyst was dried for subsequent reuse.

1.5. Natural sunlight-driven experiments

On July 26, 2025, an outdoor sunlight-driven photocatalytic conversion of xylose to xylonic acid and CO was performed on the lawn in front of the School of Art and Design, Dalian University of Technology (Liaoning, China). The experiment commenced at 11:00 Beijing Time using a large-scale sun-tracking reactor system. Prior to initiating the reaction, a 1.0 L high-pressure reactor was charged with 4.5 g of xylose and 880 mL of 0.20 M KOH solution. Then, 50 mg of the H/C-15 catalyst, after ultrasonic pretreatment, was dispersed in 20 mL of deion water to form a suspension, which was added to the reactor. The system, equipped with a solar radiation sensor, Fresnel lens, sapphire viewport, and uninterruptible power supply, and featuring a sun tracker (pointing accuracy: ±0.1°), commenced reaction upon automatic solar focusing. The reaction mixture was subjected to continuous magnetic stirring at 500 rpm for 2 h. Product analysis was conducted by GC (gaseous products) and HPLC (liquid products).

1.6. Fitting of decay curves for time-resolved photoluminescence (TRPL) spectra

These spectra can be well-fitted through a triple exponential function [1].

$$\tau_a = (A_1\tau_1^2 + A_2\tau_2^2 + A_3\tau_3^2)/(A_1\tau_1 + A_2\tau_2 + A_3\tau_3)$$

Where A_1, A_2, and A_3 represent the pre-exponential factors, τ_1, τ_2, and τ_3 signify the lifetime (ns) of various processes.

1.7. Products analysis

Post-reaction, the sample was filtered through a Millipore membrane (0.22 μm) and analyzed by high-performance liquid chromatography (HPLC) using a Bio-Rad Aminex HPX-87H column (300 mm × 7.8 mm, 9 μm). The concentrations of xylose,

lactic acid, formic acid, acetic acid, and glyceraldehyde were determined by a refractive index detector (RID-10A). The concentration of xylonic acid was measured using a variable wavelength detector (VWD) set at 210 nm. The mobile phase consisted of 5 mmol/L H_2SO_4 delivered at a flow rate of 0.5 mL/min. The column temperature was maintained at 55 ^oC, and the total analysis time per sample was 30 min. The conversion of xylose and the yield of products were calculated according to the established equations.

$$\text{Conversion}\ (\%) = \frac{\text{Moles of carbon in feedstock consumed}}{\text{Moles of carbon in feedstock input}} \times 100\%$$

$$\text{Product yield}\ (\%) = \frac{\text{Moles of carbon in organic acid}}{\text{Moles of carbon in feedstock input}} \times 100\%$$

Carbon monoxide (CO) was analyzed by gas chromatography (GC-7900) equipped with a flame ionization detector (FID) and a 5Å molecular sieve column, using argon as the carrier gas. The injector temperature was set at 110 ^oC, the column temperature was maintained at 60 ^oC, and the detector temperature was set at 200 ^oC.

2. Results and discussion

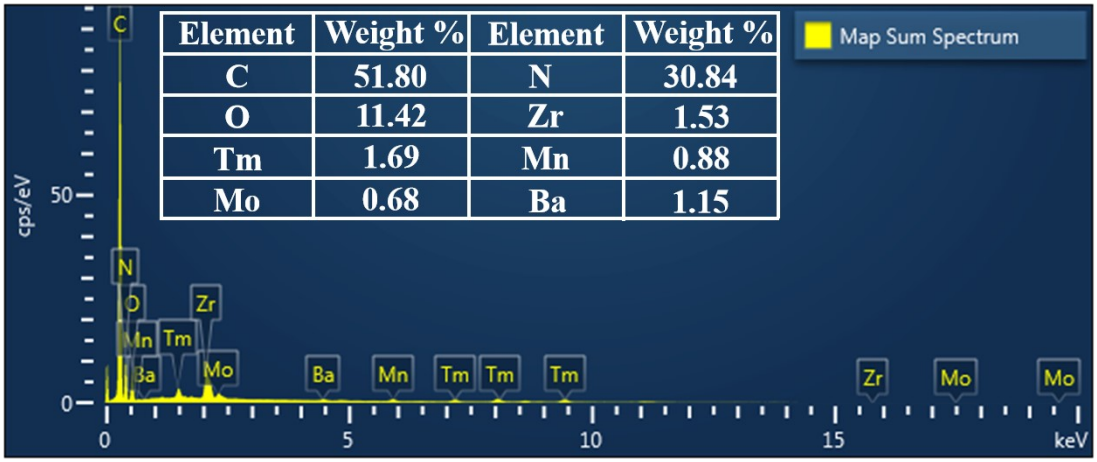

Fig. S1. EDX spectrum of H/C-15.

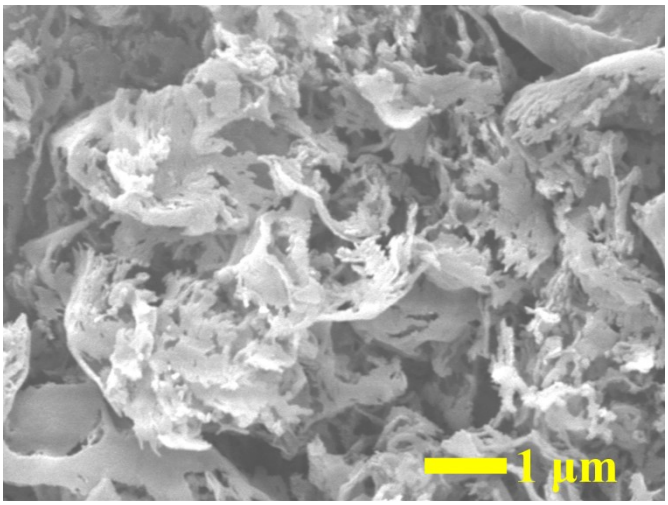

Fig. S2. SEM image of CN.

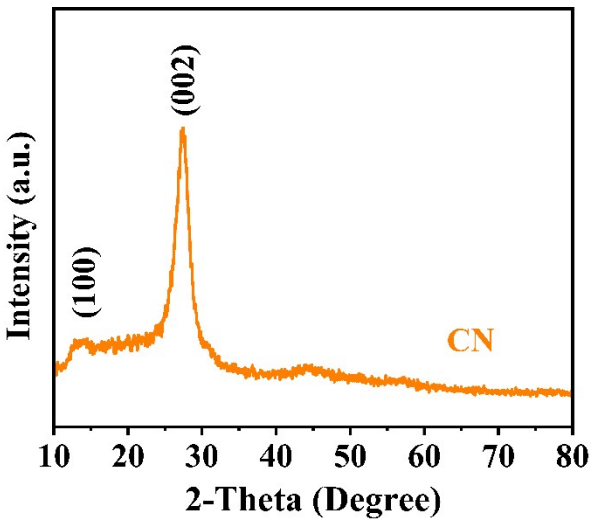

Fig. S3. XRD pattern of CN.

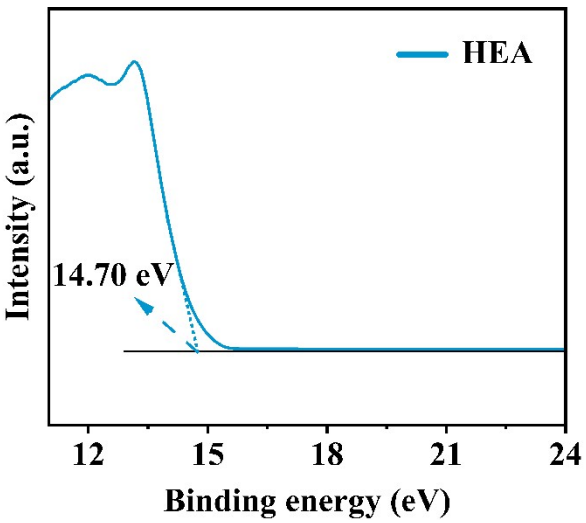

Fig. S4. HEA of UPS spectrum.

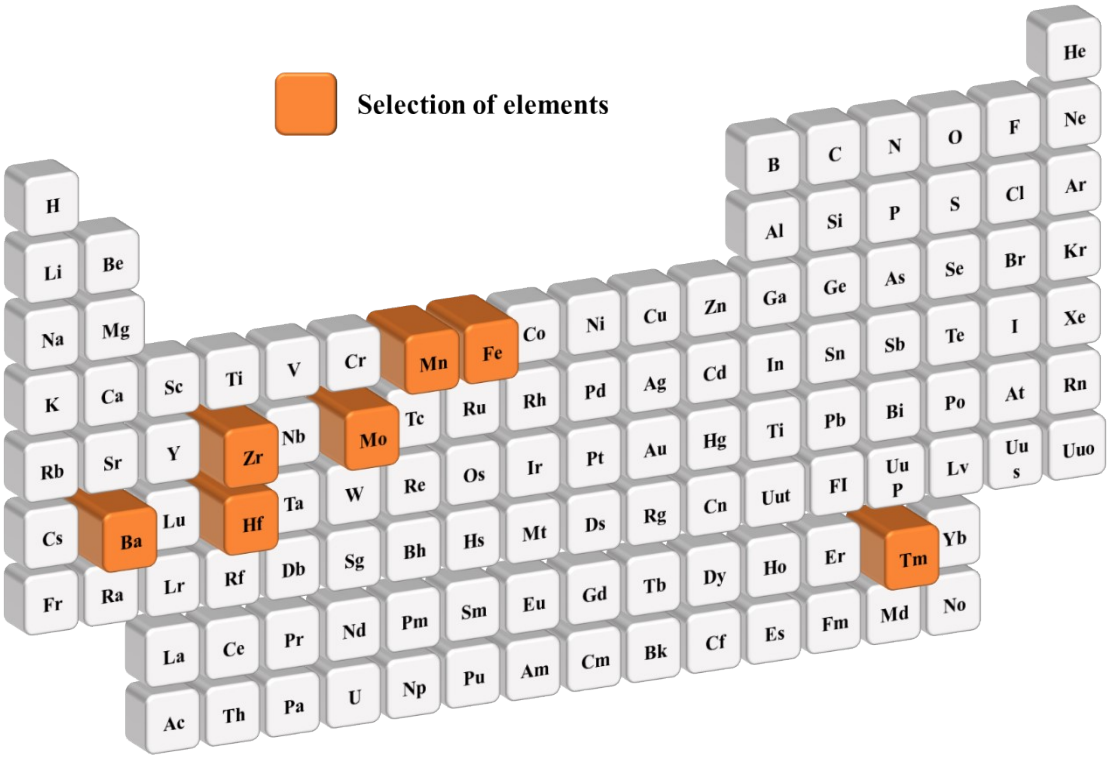

Fig. S5. Schematic diagram for selecting HEA elements.

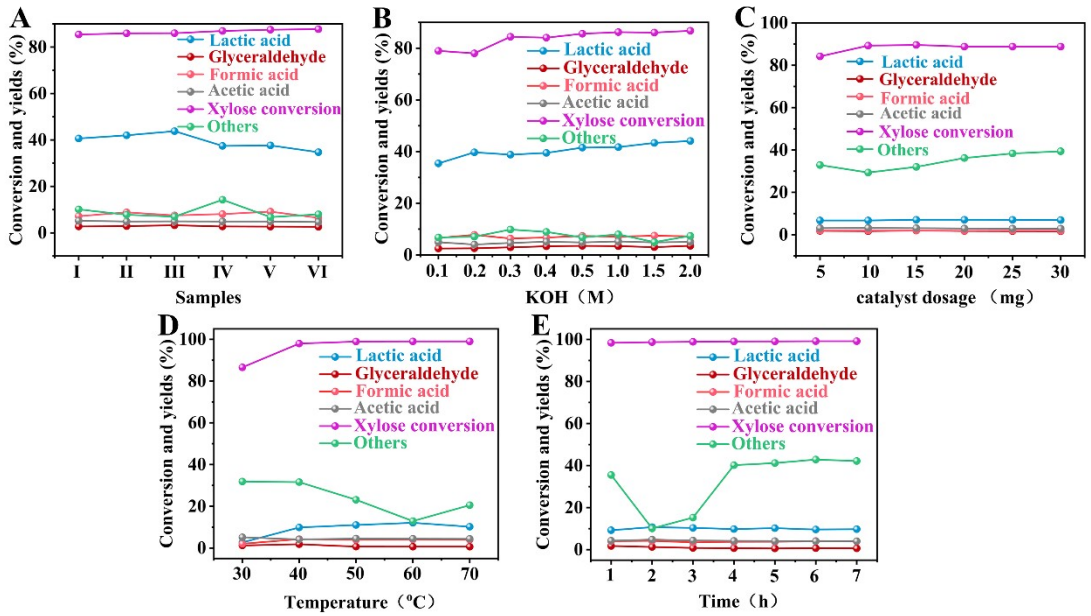

Fig. S6. Screening of different reaction conditions (A) different samples (xylose: 200 mg, photocatalysts: 10 mg, irradiation time: 3 h, reaction temperature: 40 °C, KOH solution: 0.5 M)(B) KOH concentrations (xylose: 200 mg, photocatalysts: 10 mg, irradiation time: 3 h, reaction temperature: 40 °C), (C) catalyst dosage (xylose: 200 mg, irradiation time: 3 h, reaction temperature: 40 °C, KOH solution: 0.2 M), (D) reaction temperature (xylose: 200 mg, photocatalysts: 10 mg, irradiation time: 3 h, KOH solution: 0.2 M), and (E) irradiation time (xylose: 200 mg, photocatalysts: 10 mg, reaction temperature: 40 °C, KOH solution: 0.2 M) for their effects on xylose conversion rate and byproduct yield during photocatalytic selective oxidation of xylose.

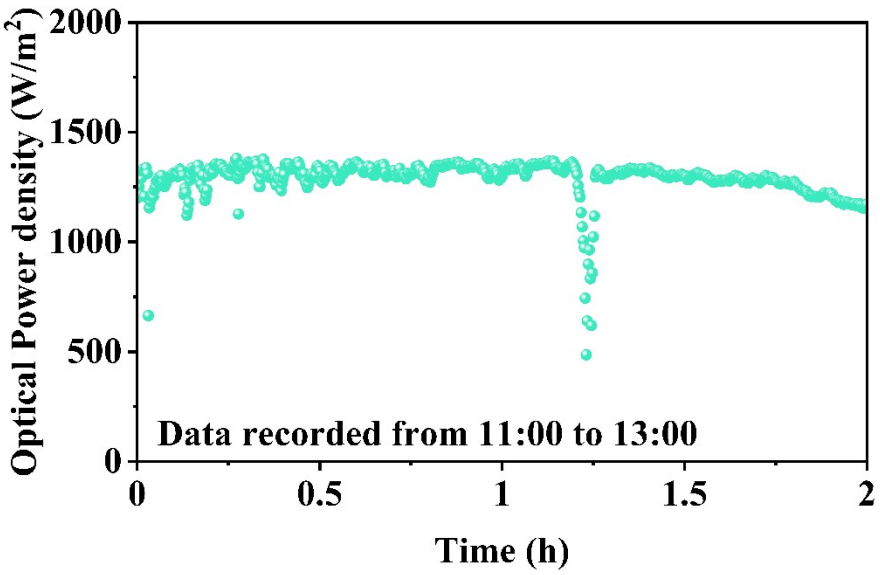

Fig. S7. Real-time optical power data collected during outdoor natural light irradiation experiment.

Table S1. The mass ratios of HEA to CN in each composite catalyst.

Samples	Theoretical ratio (%)	Actual ratio (%)
H/C-5	2.23	2.18
H/C-10	4.37	4.21
H/C-15	6.42	6.26
H/C-20	8.38	8.14

Table S2. The atomic ratio of HEA and H/C-X from ICP-OES.

Sample	Mo (at %)	Ba (at %)	Mn (at %)	Zr (at %)	Tm (at %)
HEA	22.81	21.31	21.66	16.53	17.69
H/C-5	18.19	21.27	21.76	20.65	18.09
H/C-10	18.44	21.43	20.59	21.82	17.69
H/C-15	18.73	21.19	20.58	21.24	18.24
H/C-20	18.02	21.00	21.17	21.90	17.88

Table S3. Atomic ratios of each element in the CN, HEA and H/C-15 XPS total spectra.

Samples	C (at %)	N (at %)	O (at %)	Mo (at %)	Ba (at %)	Mn (at %)	Zr (at %)	Tm (at %)
CN	50.57	47.50	1.93	-	-	-	-	-
HEA	46.06	-	38.68	3.02	3.12	3.05	2.93	3.14
H/C-15	50.14	25.20	18.39	1.18	1.25	1.23	1.32	1.29

Table S4. The average fluorescence lifetime of CN, HEA and H/C-15.

Samples	τ_1 (ns)	τ_2 (ns)	τ_3 (ns)	$\tau_{av.}$ (ns)
H/C-15	0.9714 (32.06%)	4.366 (50.88%)	20.61 (26.92%)	7.59
CN	0.8349 (20.05%)	3.536 (53.03%)	24.56 (17.06%)	3.43

Table S5. Comparison of photocatalytic xylonic acid production performance of other reported photocatalysts under visible light.

Entry	Photocatalyst	Xylonic acid （%）	Reference
1	H/C-15	67.86	This work
2	$ZnS@Bi_2S_3$	74.2	[2]
3	CIS@FSM	65.05	[3]
4	$g\text{-}C_3N_x$	64.3	[4]
5	TiO_2/Ti_3C_2	64.2	[5]
6	Pt/C	64	[6]
7	La（FeCoNiCrMn）O_3	63.9	[7]
8	$AgInS_2@CeO_{2-x}$	60	[8]
9	C-s-ZIS/CN	58.5	[9]
10	NC-800	57.4	[10]
11	Pt-HT	54	[11]
12	$3\text{-}CoSe_2/g\text{-}C_3N_4$	50.12	[12]

References

[1] C.F. Huang, L. Xiang, Y. Zhou, W.P. Xu, H.H. Mao, F.G. Qi, X.P. Ouyang, Defect assisted strong interfacial interaction in $ZnIn_2S_4/WSe_2$ heterojunction for efficient Photohydrogen production from seawater, Chem. Eng. J. 493 (2024) 152729.

[2] M.S. Li, L.X. Zhong, W. Chen, Y.M. Huang, Z.X. Chen, D.Q. Xiao, R. Zou, L. Chen, Q. Hao, Z.H. Liu, R.C. Sun, X.W. Peng, Regulating the electron–hole separation to promote selective oxidation of biomass using $ZnS@Bi_2S_3$ nanosheet catalyst, Appl. Catal. B-Environ. Energy 292 (2021) 120180.

[3] K.N. Liu, Z.D. Liu, S.Q. Yao, S.L. Sun, J.L, Ma, R.C. Sun, $CuInS_2$ quantum dots anchored onto the three-dimensional flexible self-supporting graphene oxide array with regulatable crystallinity and defect density for efficient photocatalytic synthesis of xylonic acid, Appl. Catal. B-Environ. Energy 316 (2022) 121573.

[4] Z.Y. Mu, R. Zou, W. Yang, J.L. Ma, Z.H. Chen, G. Shi, J. Liu, T.Z. Li, Y.P. Liu, X.W. Peng, g-C_3N_x with a Tunable Band Structure for Efficient Photocatalytic Xylose Oxidation and Hydrogen Evolution, ACS Sustainable Chem. Eng. 11 (2023) 10233-10241.

[5] L. Chen, Y.M. Huang, R. Zou, J.L. Ma, Y.Y. Yang, T.Z. Li, M.S. Li, Q. Hao, H.B. Xie, X.W. Peng, Regulating TiO_2/MXenes catalysts to promote photocatalytic performance of highly selective oxidation of d-xylose, Green Chem. 23 (2021) 1382-1388.

[6] S. Sadula, B. Saha, Aerobic Oxidation of Xylose to Xylaric Acid in Water over Pt Catalysts, ChemSusChem 11 (2018) 2124-2129.

[7] A.H. Li, J.L. M, M. Hong. R.C. Sun, Enhanced CeO_2 oxygen defects decorated

with $AgInS_2$ quantum dots form an S-scheme heterojunction for efficient photocatalytic selective oxidation of xylose, Appl. Catal. B-Environ. Energy 348 (2024) 123834.

[8] M.C. Wang, L.M. Li, Y. Li, X.X. Shi, H.X. Ren, Y.T. Sun, K.N. Liu, W. Song, H.M. Li, H.B. Wang, M. Han, X. Wang, C.D. Momo, S.H. Chen, L.H. Liu, H.Y. Liang, Entropy engineering of La-based perovskite for simultaneous photocatalytic CO_2 reduction and biomass oxidation, Chem. Commun. 59 (2023) 14673-14676.

[9] K.N. Liu, J.Q. Zhang, J.L. Ma, R.C. Sun, Efficient photocatalytic conversion of xylose to co-produce xylonic acid and CO via a dual S-scheme heterojunction photocatalyst between carbon nitride and $CuInS_2$ quantum dot-sensitized $ZnIn_2S_4$ Green Chem. 26 (2024) 2893.

[10] A Tathod, T Kane, E.S. Sanil, P.L. Dhepe, Solid base supported metal catalysts for the oxidation and hydrogenation of sugars. J. Mol. Catal. A-Chem. 388-389 (2014) 90-9.

[11] Z. Li, Y. Huang, X. Chi, D. Li, L. Zhong, X. Li, C. Liu, X. Peng, Biomass-based N doped carbon as metal-free catalyst for selective oxidation of D-xylose into D-xylonic acid, Green Energy Environ. 7 (2022) 1310-1317.

[12] Q. Hao, Y.J. Liu, R. Zou, G. Shi, S.L. Yang, L.X. Zhong, W. Yang, X. Chi, Y.P. Liu, S. Admassie, X.W. Peng, g-C_3N_4 nanosheets coupled with $CoSe_2$ as co-catalyst for efficient photooxidation of xylose to xylonic acid, Green Energy Environ. 10 (2025) 231-238.